THE EFFECT OF Cu AND Co CONTENT ON Ni-P-Cu-Co ELECTROPLATING BY RESPONSE SURFACE METHOD

M. H. XIAO, Z. X. HUA, Z. M. SUN, Y. X. WANG, K. CHEN, H. M. YANG[*]
College of Engineering, Nanjing Agriculture University, Nanjing 210031, China

In order to improve the organizational performance of Ni-P-Cu-Co chemical plating layer, the response surface center combined experiment was conducted to establish a mathematical model for analysis, with Cu and Co as the main index of variation. The impact of the content of Cu and Co on the microhardness and corrosion resistance of the chemical plating layer was explored, so as to obtain the optimal concentration combination. The results showed that the coating had the highest microhardness, best corrosion resistance and best comprehensive performance when the concentration of Cu and Co was combined into 18g/L of cobalt sulfate and 4g/L of copper sulfate.

1. Introduction

At present, deposition of metal plating from solution can be realized only by electroplating and electroless plating. Featuring uniform plating, flexible substrate form and strong capacity of binding plating to substrate, electroless plating has been widely used. Due to high hardness and high anti-corrosion performance, the Ni-P alloy plating has become an important surface function material [1-8]. As the Ni-P plating has been applied in more and more fields, the requirements for its performance is improving. Introducing other metal elements (such as Ni-W-P [9-12], Ni-P-B [13], Ni-Sn-P [14], etc.) to the original Ni-P plating is one of the effective methods to make it a multi-element electroless plating.

Relevant studies have shown that the introduction of Cu or Co element in the preparation of Ni-Cu-P [15-16] alloy and Ni-Co-P [17-21] alloy help them combine the advantages of Ni-P, Co-P and Cu-P and thus have excellent abrasive resistance and corrosion resistance.In the preparation of the Ni-Cu-P alloy on ZK61M Mg alloy as the substrate, Liu Junjun et al. [22] found that the introduction of the Cu element into the Ni-P plating gave the resulting Ni-Cu-P plating better corrosion resistance, and that the Ni-Cu-P plating became denser and had a higher degree of crystallization with the increase of the Cu content. They also discovered that the addition of the Cu element to the Ni-Cu-P plating contributed to the formation of the passivation film that could protect the substrate with a higher Cu content. Similarly, C. Ma et al.[23]   prepared the Ni-P-Co plating based on electrodeposition method by combining the precipitation hardening of the Ni-P

---

[*] Corresponding author: huaxmao@qq.com

alloy and the lubrication of Co. Focusing on the evaluation laws of the composition, microstructure, hardness, thermal stability and tribological properties of this alloy, they observed that the prepared Ni-P-Co plating outperformed hard chromium plating in terms of abrasive resistance and friction coefficient.

There are only a few studies on the preparation of Ni-Cu-Co-P alloy. For this regard, we made a surface response analysis (RSA) in the current study. By adding different amounts of Co and Cu into the modified plating solution, we prepared the Ni-Cu-Co-P electroless plating on 45# steel substrate. Experiments were carried out on the typical test points based on the central combination design. Starting with microhardness and corrosion current density, we fitted the relationship between factors and results to obtain the optimal combination values. The optimal proportions of the two metal elements of Cu and Co were analyzed by using Design Expert to achieve the ultimate goal of optimizing the Ni-Cu-Co-P electroless plating. The influences of the contents of Cu and Co on the Ni-Cu-Co-P electroless plating were explored to obtain the Ni-Cu-Co-P electroless plating with the best performance and the optimal proportions of Cu and Co.

2. Experiment

2.1. Preparation of the Ni-P-Cu-Co chemical plating

45# steel sheet (20mm×20mm×6mm) was selected as the plating piece. The plating solution was composed of 25g/L $NiSO_4·6H_2O$, 15-18g/L $CoSO_4·7H_2O$, 1-4g/L $CuSO_4$, 22g/L $NaH_2PO_2·H_2O$, 92g/L $NaKC_4H_4O_6·4H_2O$, 24g/L $C_{10}H_{14}N_2Na_2O_8·2H_2O$, 32g/L$(NH4)_2SO_4$ and 0.06g/L $C_{12}H_{25}SO_4Na$. The plating process lasted for 2h at (88±2)℃ (pH8.0±0.5).

2.2. Performance test of the Ni-P-Cu-Co chemical plating

(1)Microhardness: HVS-1000 digital display microhardness tester was employed to test the surface hardness of the sample with a load of 100g and hold time of 15s in 5 typical positions evenly distributing in the plating piece. The results of the five points were averaged.

(2)Corrosion resistance: Corrosion resistance was detected by CS series chemical workstation with 3.5% NaCl (wt%) as the corrosive medium. Pre-corrosion in 0.5h solution was carried out before formal detection.

2.3. Optimization of the experimental design

In this experiment, the optimal contents of element Cu and Co in the Ni-P-Cu-Co plating were analyzed to achieve the optimal performance of the plating. Thus, the two factors of $CuSO_4$ (1, 2.5, 4g/L) and $CoSO_4$ (15, 16.5, 18g/L) were selected in this experiment. Considering the obvious interaction between Cu and Co, response surface methodology (RSM) based on a central composite design (CCD) was applied by using Design-Expert 8.0.6.1. With microhardness, corrosion current density and corrosion potential as the response values, the regression model was solved and analyzed to obtain the optimal concentration combination. Table 1 shows the code and factor levels of the experimental design.

Table 1. The level of experimental factors based on response surface methodology.

Variable	Unit	Level				
		-alpha	-1	0	+1	alpha
A : CoSO4	g/L	14.37868	15.00	16.50	18.00	18.62132
B : CuSO4	g/L	0.37868	1.00	2.50	4.00	4.62132

2.4. Phase analysis and morphology of the Ni-P-Cu-Co chemical plating

The Ni-P-Cu-Co chemical plating was obtained at the optimal combined concentrations. An phase analysis was carried out on the plating by Panalytical X'PertPowder X-ray Diffractometer (incident ray: Cu Kα ray; step length: 0.02°; incidence ray: $10° \sim 90°$); the metalloscope structure on the plating surface was observed by ZEISS metalloscope, and the microstructure was observed by FMI scanning electron microscope.

3. Results and discussion

3.1. Building the regression model

Table 2 presents the experiment design and three response values. Response surface analysis (RSA) was applied to fit the unknown function relationship within the given area based on a simple mathematic model, so as to determine the relationship between each designed variable and the corresponding response value and get the optimal solution of the target function [24-25]. The data listed in Table 2 were modelled through regression by using Design-Expert 8.0.6.1, and we obtained the following multivariable regression equations regarding the correlations of $CuSO_4$ and $CoSO_4$ concentrations with microhardness, corrosion current density and corrosion potential:

$$R1=+319.97+63.05A+20.02B+54.14AB+51.05A^2-13.47B^2 \tag{1}$$

$$R2=+0.016+3.358E\text{-}004A-9.953E\text{-}005B-2.216E\text{-}003AB-2.429E\text{-}003A^2-1.387E\text{-}003B^2 \tag{2}$$

$$R3=+0.63110-0.23853A-0.11625B+0.000688889AB+0.00701111A^2+0.023656B^2 \tag{3}$$

where positive items are conducive to hardness, corrosion current density and corrosion potential (synergistic effect [26]), while negative items have an inhibitory effect on them (antagonistic effect).

530

Table 2. The experimental design matrix and results.

Run SN	A：CoSO$_4$（g/L）	B：CuSO$_4$（g/L）	Hardness（HV）	Corrosion Current Density	Corrosion Potential（V）
1	15	1	210.382±16.741	0.011645	-1.4696
2	18	1	237.244±17.104	0.016018	-1.4738
3	15	4	106.646±5.725	0.014498	-1.439
4	18	4	350.056±6.086	0.010007	-1.437
5	14.37868	2.5	470.784±39.924	0.01017	-1.4427
6	18.62132	2.5	636.32±63.475	0.012153	-1.4873
7	16.5	0.37868	371.098±20.032	0.012411	-1.4231
8	16.5	4.62132	477.936±57.785	0.014081	-1.3571
9	16.5	2.5	319.77±49.062	0.016439	-1.5102
10	16.5	2.5	321.48±6.168	0.016439	-1.5102
11	16.5	2.5	319.62±23.751	0.016439	-1.5102
12	16.5	2.5	318.98±48.648	0.016439	-1.5102
13	16.5	2.5	320.01±32.346	0.016439	-1.5102

3.2. Credibility analysis and variance analysis of the model

Whether the experimental results are reasonable mainly depends on error statistical analysis when it comes to the model credibility, including the most important correlation coefficient, variable coefficient and signal to noise ratio (SNR). The higher the correlation coefficient, the higher and more similar the corrected correlation coefficient and the predicted correlation coefficient will be, suggesting that the correlation is good, and the regression model can fully explain the experiment. A variation coefficient <10 suggests that the experimental credibility and precision are high, and a SNR>4 indicates the reasonability of the experiment. It can be seen from Table 3 that the model-based predicted values and actual values of the corrosion current density and corrosion potential are highly correlated; the regression model provides an adequate explanation; and the credibility and precision of the experiment are high. The difference between the corrected correlation coefficient of hardness and the predicted value is moderate, meaning that the model can explain this experiment. The variation coefficient (41.36) is large and the SNR is small (2.602). This suggests that the experimental precision remains low, while the mutation rate is moderate.

Table 3. The results of the model reliability analysis.

Response	Correlation Coefficient	Corrected Correlation Coefficient	Predicted Correlation Coefficient	Variable Coefficient	SNR
Hardness	0.3245	-0.1580	-3.8034	41.36	2.602
Corrosion Current	0.9174	0.8584	0.4127	6.72	9.740
Corrosion Potential	0.9218	0.8660	0.4441	1.16	11.635

Table 4 through 6 present the variance analysis of each response model. A large F value and a small p value reflect the significance of the correlation coefficient. P<0.05 is considered to suggest high model credibility. It can be seen that the models of R2 and R3 fit well in the regression region studied, so they are suitable for predicting the effects of the currently set variables on response; however, the R1 model generally shows a low degree of fitting significance, and the location of extreme point can be predicted roughly, however, there is a great difference between the predicated value and the actual value. Each p value reflects the significance of the effect on the corresponding response. A smaller p value means a high degree of significance. It can be noted that the concentration of $CoSO_4$ has the most significant impact on hardness and corrosion current density, while that of $CuSO_4$ has the most significant effect on corrosion potential.

Table 4. ANOVA of the response surface quadratic regression model for microhardness.

Item	Sum of Squares	Freedom	Mean Square Sum	F	p
Regression Model	67726.15	5	13545.23	0.67	0.6577
A-$CoSO_4$	31799.30	1	31799.30	1.58	0.2492
B-$CuSO_4$	3206.71	1	3206.71	0.16	0.7018
AB	11723.26	1	11723.26	0.58	0.4704
A^2	18130.74	1	18130.74	0.90	0.3743
B^2	1261.38	1	1261.38	0.063	0.8096
Residual	1.410E+005	7	20139.43		

Table 5. ANOVA of the response surface quadratic regression model for corrosion current density.

Item	Sum of Squares	Freedom	Mean Square Sum	F	p
Regression Model	6.98E-005	5	1.4E-005	15.55232	0.0011
A-$CuSO_4$	9.02E-007	1	9.02E-007	1.005298	0.3494
B-$CuSO_4$	7.93E-008	1	7.93E-008	0.088323	0.7749
AB	1.96E-005	1	1.96E-005	21.8901	0.0023
A^2	4.11E-005	1	4.11E-005	45.74698	0.0003
B^2	1.34E-005	1	1.34E-005	14.91263	0.0062
Residual	6.28E-006	7	8.97E-007		

Table 6. ANOVA of response surface quadratic regression model for corrosion potential.

Item	Sum of Squares	Freedom	Mean Square Sum	F	p
Regression Model	0.0240	5	4.81E-003	16.51	0.0009
A-CoSO$_4$	0.0005	1	5.33E-004	1.83	0.2183
B-CuSO$_4$	0.0032	1	3.23E-003	11.09	0.0126
AB	0.0000	1	9.61E-006	0.033	0.861
A^2	0.0017	1	1.73E-003	5.95	0.0449
B^2	0.0200	1	2.00E-002	67.69	< 0.0001
Residual	0.0020	7	2.91E-004		

Fig. 1 and 2 are the normal distribution plots of microhardness residual error and the distribution plot of residual error and predicted value, respectively. The data points in the normal distribution plot of residual error are in linear distribution, indicating that the experimental data follow the normal distribution, almost with no mutation data. The distribution plot of residual error and predicted value is irregular, suggesting that the R1 function model fitting follows the normal distribution and the experimental data are accurate.
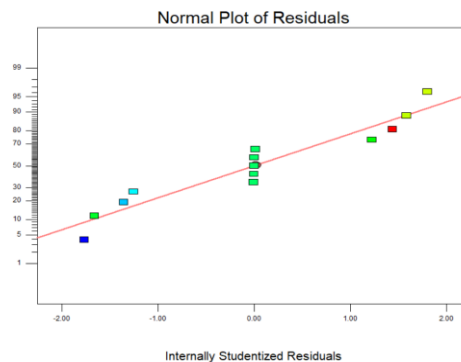
Fig. 1. The distribution plot of residuals
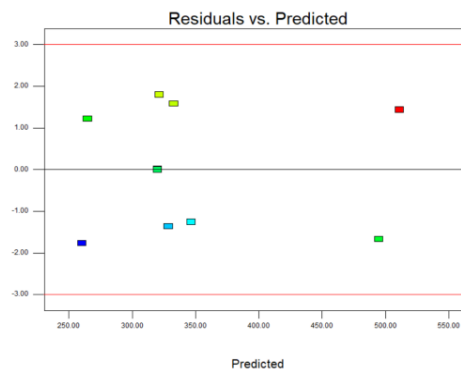
Fig. 2. The distribution plot of predicted values.

3.3. Response surface analysis

The response surface contour of microhardness is shown in Fig. 3. When the concentration of $CoSO_4$ is relatively small and the content of $CoSO_4$ keeps constant, the microhardness goes up and then declines with the consternation of $CuSO_4$. This reveals that the facilitating role of $CuSO_4$ on the precipitation of the three metals enhances excessively and then weakens within a certain range. When the concentration of $CoSO_4$ is relatively large, the contour tends to be perpendicular to the coordinate axis of $CoSO_4$, revealing that item A in the variance analysis ($CoSO_4$) has the most significant impact on R1 (P value reaches the minimum), which is considered to be caused by the large hardness of Cu element. When the concentration of $CuSO_4$ is constant, the hardness will significantly increase with the concentration of $CuSO_4$ in a steady way (step value=50, with a similar contour distance). The tendency of the contour line shows that within a given range of factor level, the hardness reaches the maximum in the right upper corner (with 18g/L $CoSO_4$ and 4g/L $CuSO_4$). It is apparent that the highest response points are at the sites where A and B reach the upper level, as shown in the 3D response surface plot of microhardness in Fig. 4.

Fig. 3. The contour map of microhardness response surface.
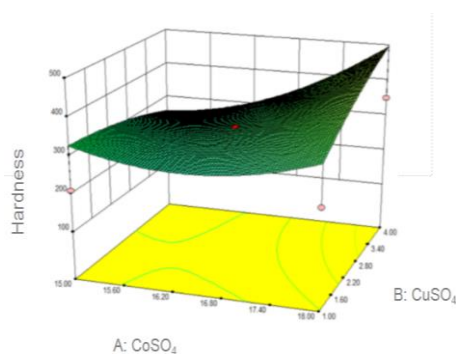
Fig. 4. The 3D diagram of microhardness response surface.

Both corrosion current density and self-corrosion potential are important factors affecting the corrosion resistance of the plating. The more positive the self-corrosion potential, the more likelihood of plating corrosion would be; the smaller the corrosion current density, the slower the corrosion is. Corrosion current density is the leading parameter to evaluate the corrosion performance of the plating [27-28].

Fig. 5 shows the response surface contour map of corrosion current density. The ellipse contour suggests a significant interaction between different factors. It can be seen from the

variance analysis that item AB has a relatively significant influence on R2, that is to say, the interaction between two factors is obvious and the contour tends to be close. When the concentration of either A or B keeps constant, R4 rises and then drops with the change of the other factor. However, when the two factors are in the upper and lower levels respectively, the corrosion current density drops (A=1 and B=1 at the optimal point, with 18g/L $CoSO_4$ and 4g/L $CuSO_4$; or A=-1 and B=-1,with 15g/L $CoSO_4$ and 1g/L $CuSO_4$).

It is noted that the minimum levels are in the two corners, as shown in the 3D view of the response surface of corrosion current density in Fig. 6.
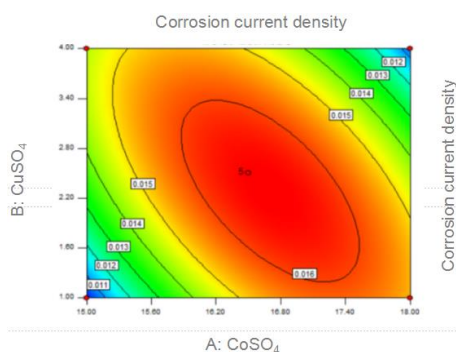
Fig. 5. The contour map of corrosion current density response surface.
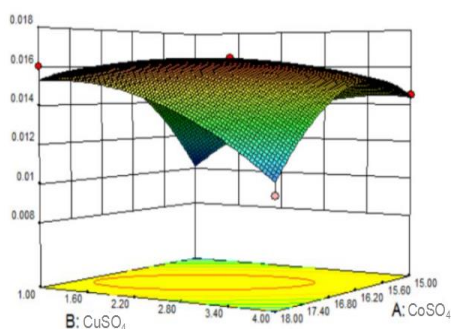
Fig. 6. The 3D diagram of corrosion current density response surface.

The response surface contour map and 3D map of corrosion potential are shown in Figs. 7 and 8 respectively. The variance analysis suggests that B and AB have the most significant impact on R5. It is evident in the contour map that when $CoSO_4$ is kept at a certain concentration, the corrosion potential turns negative and then positive with the increase in the concentration of $CuSO_4$; when the $CaSO_4$ concentration is constant, the corrosion potential has no obvious change within this range, indicating the effect of B on R5. The contour map and 3D view 3-36 show that the $CuSO_4$ concentration equals to the upper level. The optimal points can be obtained when A=-1 and B=1 (15g/L $CoSO_4$ and 4g/L $CuSO_4$) and when A=1 and B=1 (18g/L $CoSO_4$ and 4g/L $CuSO_4$).
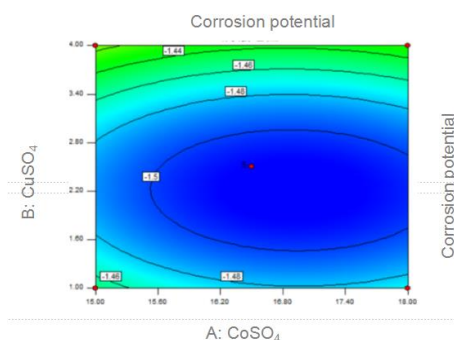
Fig. 7. The contour map of corrosion potential response surface.
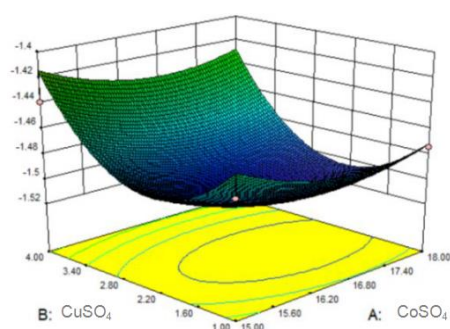
Fig. 8. The 3D diagram of corrosion potential response surface.

To sum up, the plating achieves the optimal comprehensive performance with 18g/L $CoSO_4$ and 4g/L $CuSO_4$.

3.4 Phase analysis and morphology of the Ni-P-Cu-Co chemical plating with the optimal combination

Fig. 9 shows the X-ray diffraction diagrams of the Ni-P-Cu-Co chemical plating with different process parameters. It can be noted that no Fe compound is found in each layer, and there are relatively sharp diffraction peaks in some layers, which may be caused by the substrate hit by X-ray due to the thin plating. When the number of cupric ions is increased appropriately, they will first promote the combination of cobalt ions and phosphonium ions and have no evident facilitating role on nickel ions. Thus, cobalt ions will deposit first and bind to phosphonium and themselves will also bind to phosphonium ions. It is apparent that there are the phosphides of the three elements and their own deposits in the plating with 18g/L $CoSO_4$ and 4g/L $CuSO_4$.
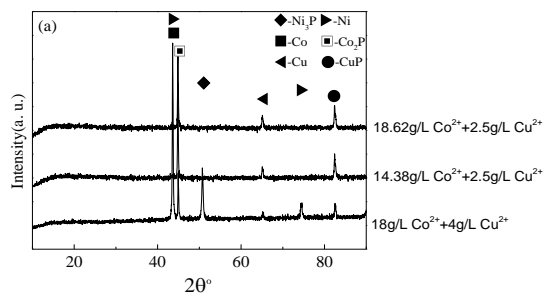
Fig. 9. The XRD diagram of the Ni-Co-Cu-P plating.

Fig. 10 shows the SEM secondary electron images and backscattered electron images of the Ni-Co-Cu-P chemical plating with 18g/L $CoSO_4$ and 4g/L $CuSO_4$ at different magnifications. Compassion of the two images allows us to observe multiple elements in the plating which are mainly in a cauliflower structure. The wrapped cubic structure is considered to be Co element, while Cu element turns into a consolidated flow texture to fill up the pores in the cauliflower structure because of its soft texture. It can be seen that the three elements of main salt are infused well and perform their own functions to form a dense plating.

a)

b)

c)

d)
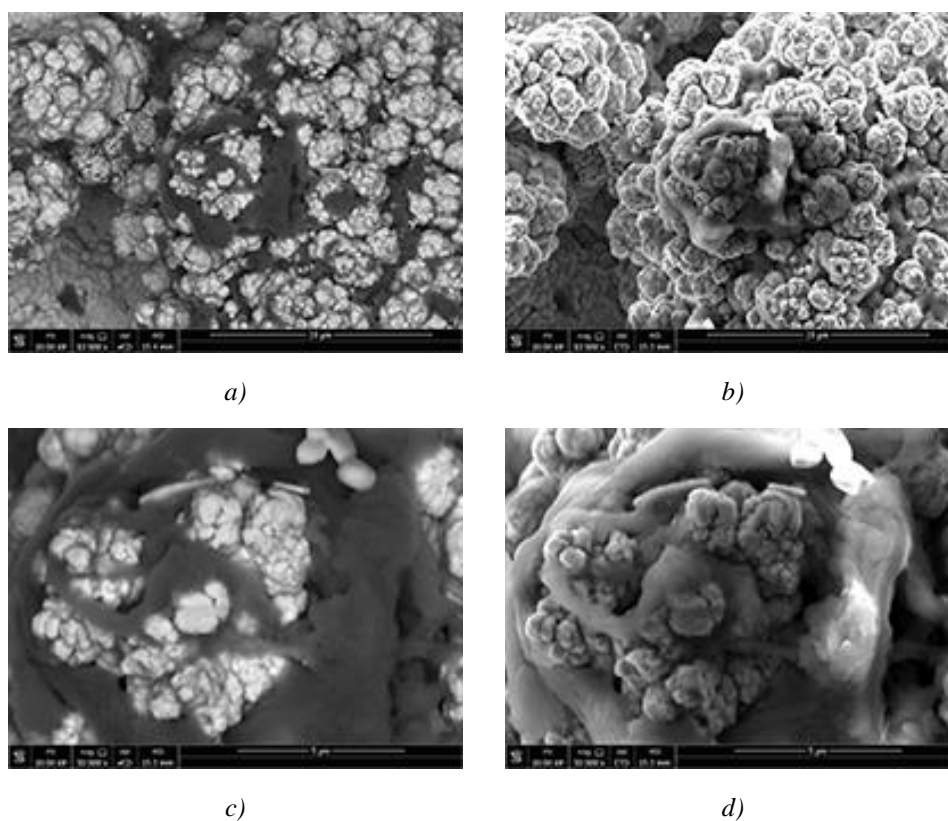
Fig. 10. The SEM secondary electron images and backscattered electron images of the Ni-Co-Cu-P chemical plating with 18g/L $CoSO_4$ and 4g/L $CuSO_4$ under different magnifications: (a) 10000 times SEM images; (b) 10000 times SEM backscattered electron images; (c) 50000 times SEM images; (d) 50000 times SEM backscattered electron images

4. Conclusions

The maximum microhardness is optimal with 18g/L $CoSO_4$ and 4g/L $CuSO_4$. In the analysis of the response surface function model, the optimal combination of surface friction coefficient and abrasion loss is obtained with 18g/L $CoSO_4$ and 4g/L $CuSO_4$.

In conclusion, the plating achieves the optimal comprehensive performance and has relatively strong abrasive resistance and corrosion resistance, and the microhardness is large with 18g/L $CoSO_4$ and 4g/L $CuSO_4$.

Data Availability

All relevant data are within the paper.

Competing Interests

The authors declare that there are no competing interests regarding the publication of this paper.

References

[1] Q. Zhao, Y. Liu, Corrosion Science **47**, 2807 (2005).
[2] G. L. Zhao, Y. Zou, H. Zhang, Z. D. Zou, Material Letters **132**, 221 (2014).
[3] B. Jiang, S. L. Jiang, A. L. Ma, Y. G. Zheng, Journal of Materials Engineering and Performance **23**, 230 (2014).
[4] Z. Rajabalizadeh, D. Seifzadeh, Protection of Metals and Physical Chemistry of Surfaces **50**, 516 (2014).
[5] P. Makkar, R. C. Agarwala, Journal of Materials Science **50**, 2813 (2015).
[6] K. Dhanapal, V. Narayanan, A. Stephen, Materials Chemistry and Physics **166**, 153 (2015).
[7] X. B. Xi, H. Miao, R. H. Zhang, J. L. Cheng, Surface and Coatings Technology **297**, 27 (2016).
[8] C. H. Wang, Z. Farhat, G. Jarjoura, M. K. Hassan, A. M. Abdullah, E. M. Fayyad, Surface and Coatings Technology **326**, 336 (2017).
[9] M. Palaniappa, S. K. Seshadri, Wear 265, 735 (2008).
[10] J. N. Balaraju, N. T. Kalavati, V. K. Manikandanath, William Grips, Surface and Coatings Technology **206**, 2682 (2012).
[11] J. N. Yang, S. C. Balaraju, H. Chong, C. Q. Xu, V. V. Liu, Z. Chen, Silberschmidt, Journal of Alloys and Compounds **565**, 11 (2013).
[12] A. Akyol, H. Algul, M. Uysal, H. Akbulut, A. Alp, Applied Surface Science **453**, 482 (2018).

[13] G. Stremsdoerfer, H. Omidvar, P. Roux, Y. Meas, R. Ortega-Borges, Journal of Alloys and Compounds **466**, 391 (2008).

[14] J. Georgieva, S. Armyanov, Journal of Solid State Electrochemistry **11**, 869 (2007).

[15] H. S. Yu, S. F. Luo, Y. R. Wang, Surface and Coatings Technology **148**, 143 (2001).

[16] Z. Rajabalizadeh, D. Seifzadeh, Protection of Metals and Physical Chemistry of Surfaces **50**, 516 (2014).

[17] D. Seifzadeh, A. Rahimzadeh Hollagh, Journal of Materials Engineering and Performance **23**, 4109 (2014).

[18] J. Yuan, J. Wang, Y. Gao, J. Mao, W. Hu, Thin Solid Films 632, **1** (2017).

[19] T. Chen, Y. Sun, M. Guo, M. Zhang, Journal of Alloys and Compounds **766**, 229 (2018).

[20] C. Ma, S. C. Wang, L. P. Wang, F. C. Walsh, R. J. K. Wood, Surface and Coatings Technology **235**, 495 (2013).

[21] L. Hou, S. Bi, H. Zhao et al., Applied Surface Science **403**, 248 (2017).

[22] J. J. Liu, X, D, Wang, Z. Y. Tian, M, Yuan, X. J. Ma, Applied Surface Science **356**, 289 (2015).

[23] C. Ma, S. C. Wang, L. P. Wang, F. C. Walsh, R. J. K. Wood, Surface and Coatings Technology **235**, 495 (2013).

[24] E. A. Patterson, M. P. Whelan, Progress in Biophysics and Molecular Biology **129**, 13 (2017).

[25] W. T. Zhao, Z. P. Qiu, Finite Elements in Analysis and Design **67**, 34 (2013).

[26] L. Guo, L. R. Xiao, X. J. Zhao et al., Ceramics International **43**(5), 4076 (2017).

[27] J. Chen, Y. Zou, K. Matsuda, G. L. Zhao, Material Letters **191**, 214 (2017).

[28] Y. Xu, X. Zheng, X. Hu et al., Surface and Coatings Technology **258**, 790 (2014).